Lumped Parameter Model for Transient Simulation of Line-Start Synchronous Reluctance Machines

Jannik RITUPER and Raimund GOTTKEHASKAMP
University of Applied Sciences Düsseldorf, Germany

ABSTRACT – Numerical models for Line-Start Synchronous Reluctance Machines are often too inaccurate or too time consuming. In previous work, a lumped parameter model with global saturation factors for the d- and q-axis, instead of large current-flux linkage lookup tables, has been introduced. It provides relatively accurate results with reasonable computing time. In this paper, this model is compared for different line-start scenarios with a transient 2D Finite Element model. The results show that the model is accurate enough to estimate the synchronization behavior of the machine under different conditions.

AC motors, analytical model, direct on line, line start, saturation factor, synchronous reluctance motor

1. INTRODUCTION

Line-Start Synchronous Reluctance Machines (LSSynRM) have long been known as a technology to replace small Induction Machines providing a fixed speed drive for various applications. During the 20th century, simple approaches such as cutting off two sides of a standard Induction Machine rotors were applied without focusing on improving efficiency. The only requirement was to start directly online and to reach synchronous speed, regardless of steady-state performance.

But the efficiency requirements for Induction Machines have increased since then [1], which has revived interest in Line-Start Synchronous Machines. While mostly Line-Start Permanent Magnet Synchronous Machines have been applied due to their high power density and efficiency, there are disadvantages to this technology: magnet prices are volatile and the extraction of the material is considered harmful to the environment. This is why the Line-Start Synchronous Reluctance Machine is once again a popular topic.

To date, however, it has been a major challenge to develop LSSynRMs that can actually replace the versatile and reliable Induction Machine. In this context, increasing efficiency is a task that can be achieved primarily through the technology's inherent absence of rotor losses in synchronous operation and a well designed rotor with maximized anisotropy to reduce the magnetization current. However, these designs are usually not suitable for accommodating a symmetrical rotor cage with sufficient conductor material near the outer diameter. Therefore, the start-up behavior is principally worse than in classical Induction Machines.

Yet, good start-up behavior is essential for an LSSynRM, since it must pull itself from asynchronous to synchronous operation. The higher the maximum asynchronous speed, the lower the energy that has to be applied by the synchronous torque and thus the higher the probability of a successful startup. This is not necessary with the Induction Machine, which is why the conflicting goals of start-up and steady-state behavior are less of an issue in the design process. It can cope with a wide variety of load torques and all inertias, while being limited exclusively by thermal constraints.

In order to meet this goal also for LSSynRMs, there are different design approaches. In theory, the topology of a LSSynRM can be derived either from an Induction Machine or from a Synchronous Reluctance Machine. The three state-of-the-art topologies are shown in Figure 1. In topology A, flux barriers (and sometimes cutoffs) are added to a squirrel cage rotor to increase the inductance difference between the d- and q-axes. Usually this leads to a good start-up behavior but a poor efficiency.

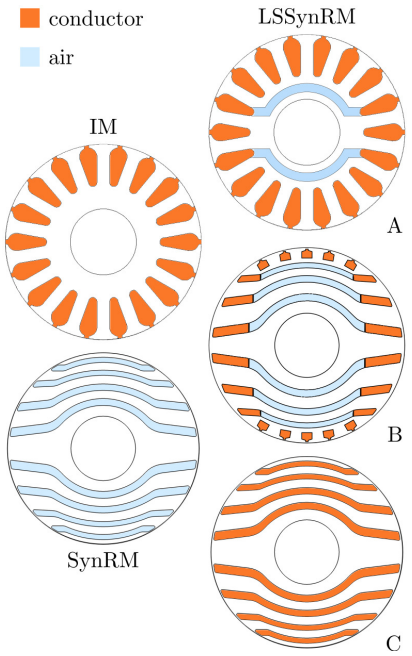

Figure 1. State-of-the-art LSSynRM rotor topology obtained from an Induction Machine or from a Synchronous Reluctance Machine (2-pole machines).

The topology C starts from a Synchronous Reluctance Machine design and adds conductors into the rotor, for example by filling the flux barriers with aluminum and adding end rings. This approach has poor start-up behavior because there is much less conductive material near the air-gap, especially along the q-axis where it is crucial to reduce resistance [2]. Even though fully filling the barriers with aluminum can help decrease the rotor resistance, this cannot completely compensate for the poorer cage geometry. This is mainly due to the fact that internal flux barrier regions near the shaft hardly carry any current anyway, even at small slip frequencies, due to shielding effects.

This is why the flux barrier design is often adapted when asynchronous torque is considered [2, 3]. This results either in redesigned flux barriers or even in a hybrid type machine, as shown in topology B, where the cage is more evenly distributed near the rotor air-gap and with more conductive material in this critical area, while decreasing the synchronous torque due to the deterioration of the d-axis magnetic flux paths and improving the q-axis ones.

This wide variety of geometries and the ever-increasing performance requirements imply the need for accurate and fast numerical models to compare different machines. To our knowl-

edge, there is no model that is fast enough and capable of reflecting a small change in geometry on the dynamic performance of the machine. Analytical models, for example, do not really cover this aspect. The much-used dq models are also often too inaccurate and the parameter calculation error-prone [4]. The only possibility seems to be the Finite Element Model (FEM) either as pure 2D or coupled circuit 2D model. Note that even 3D models have been used for specific LSSynRM [5]. But since the design and optimization processes often require thousands of simulations the use of FEM is impractical.

In a previous work a lumped parameter model for simulating LSSynRM with Induction Machine type cages [6, 7] has been developed, where the parameters are calculated by finite element analysis and stored in lookup tables. The initial value problem is then solved numerically, providing fast and accurate results. While this approach is a good start, it still has weaknesses and needs to be improved to be adapted to different types of LSSynRM.

On the one hand, the saturation model implemented in the model is not accurate enough for Synchronous Reluctance Machines because it oversimplifies the saturation state of a machine by neglecting its anisotropy. On the other hand, the use of skin effect factors for resistance and inductance fitting only accounts for standard Induction Machine slots. This is not applicable for LSSynRM with conductors in flux barriers. The approach of filling flux barriers or parts of it as well as other non-standard slot geometries with conductive material also provides new challenges for the formulation of the model.

In this context, we introduce here an improved LSSynRM lumped parameter model. It is applicable for any topology of Line-Start Synchronous Reluctance Machines. To model the saturation, a two factor approach is introduced to account for the different saturation states of d- and q-axes [8]. The skin effect is considered by introducing a layer approach that divides the rotor cage into several distinct cages.

The paper is organized as follows: in section 2 the lumped parameter model is derived while clarifying the improvements over the previous model of [6, 7]. The calculation of the parameters will also be briefly explained. Section 3 shows the simulation results compared to FEM for a 2-pole Line-Start Synchronous Reluctance Machine. The paper concludes with a discussion of the results.

2. LUMPED PARAMETER MODEL

2.1. *Linear model*

The voltage equation for the k-th stator phase is:

$$u_\mathrm{k} = R_\mathrm{ph,k} i_\mathrm{k} + \frac{\mathrm{d}}{\mathrm{d}t} \sum_{k'=1}^{m} \psi_\mathrm{k,k'} + \frac{\mathrm{d}}{\mathrm{d}t} \sum_{j'=1}^{N_\mathrm{loops}} \psi_\mathrm{k,j'}. \tag{1}$$

where $R_\mathrm{ph,k}$ is the phase resistance, i_k the phase current, and $\psi_\mathrm{k,k'}$ and $\psi_\mathrm{k,j'}$ the flux linkages caused by the k'-th stator phase and the j'-th rotor loop, respectively.

For the N_loops rotor loops, however, the derivation of a circuit model may seem quite unclear at a first glance. In a typical Induction Machine, the cage geometry is symmetrical for each rotor slot pitch and all rotor bars are identical. It is therefore easy to divide the cage into multiple equal loops, each consisting of two neighboring bars and the two linking ring segments.

The rotor cage of modern LSSynRM however is more complex (see Fig. 1). For the type where the conductors are placed in the flux barriers, neighboring rotor bars are different. The loops consisting of each two bars are also affected by the rotor's anisotropy. Therefore, the rotor cage needs a new definition of bars and ring segments which form loops in order to develop a circuit model and to define the parameters. The approach has already presented in [9] and will be briefly clarified again.

It is most practical to stay as close to an Induction Machine as possible because the behavior is quite similar and the calculation techniques could stay the same as well. As shown in Figure 2, the conductors are counted around the rotor surface, which leads to defining each 'wing' of a flux barrier, i.e. one of the symmetric sides, as one rotor bar. One rotor loop therefore consists of two neighboring rotor bars again (i.e. 1 and 2, 2 and 3, etc.).

What stands out is that most loops produce and enclose flux that passes through the iron paths between two flux barriers, i.e. the d-axis (e.g. loop of the rotor bars 1 and 2). But there is one loop per pole which consists of the two identical sides of the outermost flux barrier (e.g. 4 and 5). This loop will produce magnetic flux in the q-axis.

We can then calculate the inductance of each loop (containing the main flux and slot leakage flux) with linear 2D static FEM as well as the resistance of both bars and still need the ring parameters for a quasi 3D model. The ring segments are easy to define as the segments connecting those bars. However, many different geometries for those segments prove the complexity of the model.

The equation for the rotor loops is then the same as known for Induction Machines with the difference that two different bar resistances have to be taken into account:

$$\begin{aligned} 0 = {} & 2R_\mathrm{r,j} i_\mathrm{r,j} + R_\mathrm{b,j} \left(i_\mathrm{r,j} - i_\mathrm{r,j-1}\right) + R_\mathrm{b,j+1} \left(i_\mathrm{r,j} - i_\mathrm{r,j+1}\right) \\ & + \frac{\mathrm{d}}{\mathrm{d}t} \sum_{k'=1}^{m} \psi_\mathrm{j,k'} + \frac{\mathrm{d}}{\mathrm{d}t} \sum_{j'=1}^{N_\mathrm{loops}} \psi_\mathrm{j,j'}. \end{aligned} \tag{2}$$

The full system of all stator and rotor equations can be also expressed in matrix form:

$$\vec{u} = \widetilde{R}\vec{i} + \frac{\mathrm{d}}{\mathrm{d}t}\vec{\psi}. \tag{3}$$

We define the inductances as constant because the saturation approach will be an additional saturation factor matrix. Hence, we achieve a matrix $\widetilde{L}$ which only depends on the rotor angle. With

$$\vec{\psi} = \widetilde{L}\vec{i} \tag{4}$$

we can replace the current vector in Eq. 3 so that the flux linkage is the unknown state variable to solve for:

$$\frac{\mathrm{d}}{\mathrm{d}t}\vec{\psi} = \vec{u} - \widetilde{R}\widetilde{L}^{-1}\vec{\psi}. \tag{5}$$

2.2. *Skin Effect*

The skin effect is important to consider because it affects the resistance and inductance of all rotor bars over the whole start-up range. This affects the fundamental rotor current, which will reach low frequencies near synchronous speed, but also harmonic currents, that will be mainly observable in synchronous operation.

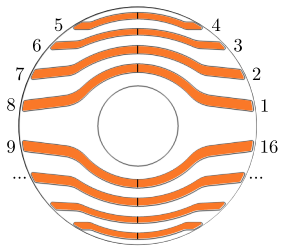

Figure 2. Definition of rotor loops in LSSynRM rotors with a rotor cage embedded in the flux barriers.

In order to have a versatile model with a good representation of the effect, the well-known layer approach has been successfully applied [9]. Here, the rotor is divided into multiple, separate cages, which provides good results for every slip. The rotor model, and thus also the system of equations in Eq. 3 introduced in the previous subsection is therefore extended. Dividing the rotor in N_L layers therefore results in $N_\mathrm{L}{\cdot}N_\mathrm{loops}$ rotor voltage equations. Figure 3 shows the rotor layers in a 4-pole LSSynRM.

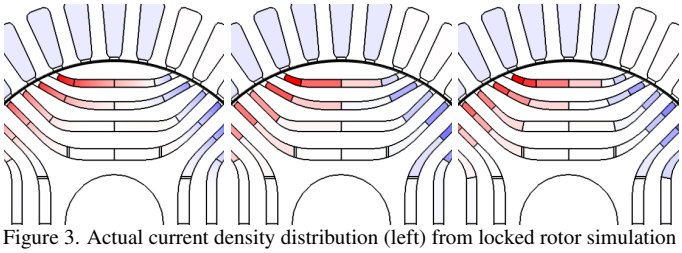

Figure 3. Actual current density distribution (left) from locked rotor simulation of a 4-pole LSSynRM and approximated current density distributions with 2 layers (middle) and 3 layers (right) with constant current density per layer.

2.3. Saturation

To consider for saturation basically means to find a function which yields the non-linear relation between current and flux linkage. Instead of functions, usually lookup tables are calculated with FEM and then interpolated for each time step in the model. In practice, this means that for many sets of currents, the flux linkage will be calculated by means of static FEA (or other methods). Usually for synchronous machines this is no big effort since there are m stator currents and no more than one rotor excitation current in wound field machines (or 4 in total for dq models) [10, 11].

In Line-Start Synchronous Reluctance Machines however, we have three currents for the stator and N_loops currents for the rotor (in this model even $N_\mathrm{L}{\cdot}N_\mathrm{loops}$). This leads to a number of variations that would cause tremendous amount of calculation time which is not practical anymore.

Hence, the saturation approach has to be simplified. In case of Induction Machines as well as for LSSynRM [6, 7] a global saturation factor has already been applied successfully. The main principle is to multiply a saturation factor Λ_sat in Eq. 4 which adapts the resulting flux linkage vector $\vec{\psi}$ depending on the current $\vec{i}$:

$$\vec{\psi} = \Lambda_\mathrm{sat}\widetilde{L}\vec{i}. \tag{6}$$

For LSSynRM this has been expanded to a two factor model, so that we have $\Lambda_\mathrm{sat,d}$ and $\Lambda_\mathrm{sat,q}$ as separate factors to consider for d- and q- axis saturation. Also every rotor loop has a saturation factor which is evaluated from both main factors. This approach is explained in detail in [12]. As a result we have a function

$$\vec{\psi} = \widetilde{\Lambda}_\mathrm{sat}\widetilde{L}\vec{i}, \tag{7}$$

where the saturation factor is now a matrix $\widetilde{\Lambda}_\mathrm{sat}$ which only depends on the stator currents. For replacing the current we use

$$\vec{i} = \widetilde{k}_\mathrm{sat}\widetilde{L}^{-1}\vec{\psi}, \tag{8}$$

where $\widetilde{k}_\mathrm{sat}$ is the inverse of $\widetilde{\Lambda}_\mathrm{sat}$. This results in the following system of equations:

$$\frac{\mathrm{d}}{\mathrm{d}t}\vec{\psi} = \vec{u} - \widetilde{R}\widetilde{k}_\mathrm{sat}\widetilde{L}^{-1}\vec{\psi} \tag{9}$$

The calculation of the lookup table for $\widetilde{k}_\mathrm{sat}$ as well as all other parameters is briefly summarized in the next section.

2.4. Parameter Calculation

2.4.1. Inductances

The stator and rotor inductances that populate the inductance matrix $\widetilde{L}$ are calculated with 2D static Finite Element Analysis with linear material. The permeability of all rotor bridges has to be set to μ_0 [9, 6]. Since the inductances depend on the rotor angle ϑ due to the anisotropy and slotting effects, the calculation has to be carried out for a sufficient amount of sample points.

The resulting inductances from FEM contain the main inductances as well as the slot leakage inductances. For the stator end winding leakage inductance of distributed windings, it is most reasonable to use known empirical formulas based on a leakage factor. The same goes for the rotor end ring leakage inductance.

2.4.2. Resistances

The stator phase resistance $R_\mathrm{ph,k}$ can be either obtained by measurements or standard formulas. The resistances of the j-th rotor bar $R_\mathrm{b,j}$ is also calculated with

$$R_\mathrm{b,j} = \frac{l_\mathrm{z}}{\kappa S_\mathrm{b,j}} \tag{10}$$

where l_z is the axial length of the rotor bar and $S_\mathrm{b,j}$ its surface which can be obtained e.g. in the FE model itself.

The rotor end ring resistances however are more complex due to the varying geometries and the 3D current distribution. They could be approximated with the same formula as in Eq. 10. However, 3D FEM as for example in [13] will be more precise and is thus used in this paper.

2.4.3. Saturation factors

The saturation factors for this model are calculated with static 2D Finite Element Analysis. At first, a 2D lookup table for $(\vec{\psi}_\mathrm{S,d}, \vec{\psi}_\mathrm{S,q})^T = f(I,\gamma)$ of a sufficient amount of steps is calculated with non-linear material conditons, i.e. the $B(H)$ curve of all non-linear materials is taken into account. I is the absolute value and γ the angle of a stator current space vector. Rotor currents are not considered. The results for the 2-pole machine from the upcoming validation section are shown in Fig. 4 as an example.

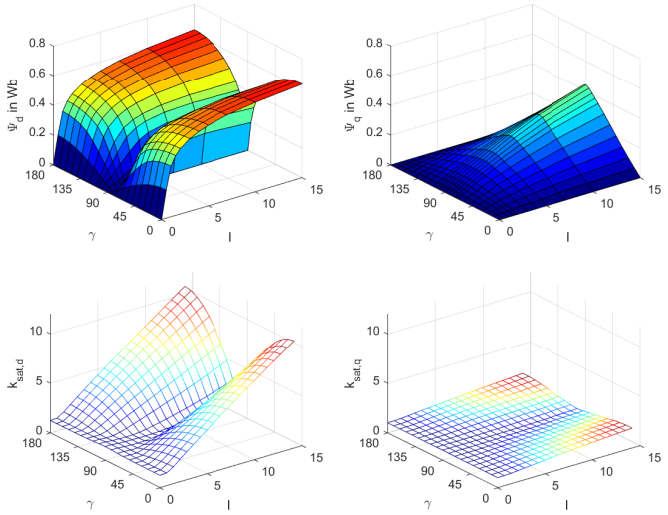

Figure 4. Top: Flux linkage components of d- and q-axes for different stator current space vectors. Bottom: Resulting saturation factors for d- and q-axes.

Then the same sample points are calculated with linear material conditions. To save time, this can also be done by using the inductance matrix (of the stator) that has already been calculated in Section 2.4.1. The saturation factors of d- and q-axes for each

sample point are then calculated by dividing the saturated by the linear value. Further explanations on how the saturation of the full model is adapted by using only stator saturation factors are given in [12].

3. RESULTS

In previous work, the model has been validated for the linear case to prove the good accuracy of the skin effect approach [9] as well as for the non-linear case with steady-state calculations [12]. Therefore, it is now necessary to investigate if the model is accurate enough to simulate a full start-up of a Line-Start Synchronous Reluctance Machine.

3.1. Machine under test

For this purpose, a 2-pole Line-Start Synchronous Reluctance Machine with IEC90 frame size is chosen. It has been designed in a research project as an initial design, which should be intentionally not optimized. This allows for better comparison of parasitic effects and poor start-up behavior because the model must be able to reproduce it. Figure 5 shows the geometry, the machine data is given in Table 1.

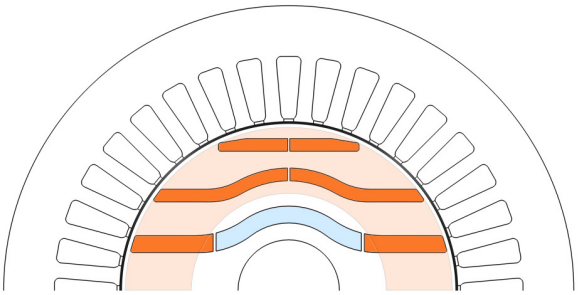

Figure 5. Geometry of the Line-Start Synchronous Reluctance Machine used for the validation. Conductive material in the rotor is indicated with orange color, air is set to light blue. The area covered by the end ring is indicated in light orange.

Table 1. Machine Data

Parameter		**Value**
Stator outer diameter	D_o	135 mm
Stator inner diameter	D_i	80 mm
Core length	l_Fe	40 mm
Air-gap width	δ_g	0.4185 mm
Number of stator Slots	Z_1	36
Number of phases	m	3
Number of poles	$2p$	2
Number of turns of a coil	N	45
Stator resistance	R_ph	4.6 Ω
Number of flux barriers	N_FB	6
Electrical steel (stator)		M250-35A
Electrical steel (rotor)		M800-50A
Rotor cage material		aluminum

3.2. Reference model

A transient 2D Finite Element Model is chosen as reference. It is implemented in COMSOL Multiphysics 5.6 ®. The mesh is shown in Figure 6. Only one pole of the machine is modelled by using antiperiodic boundary conditions. The stator windings as well as the rotor cage are implemented as electrical circuits which are coupled with the 2D model by voltage sources providing the EMF. The nonlinear material is taken into account by the $B(H)$ curves from the manufacturer. For start-up simulation, sine voltage sources supply the stator circuit and the equation of motion is programmed as additional ODE to account for the dynamic behavior. In this work, only the case of the uncoupled machine running up against its own friction torque of 0.05 $\mathrm{N{\cdot}m}$ and its own inertia of approximately 0.0012 $\mathrm{kg{\cdot}m^2}$ is investigated. The time step for solving the initial value problem is chosen to 40 µs which is 500 steps per cycle at the chosen frequency of 50 Hz.

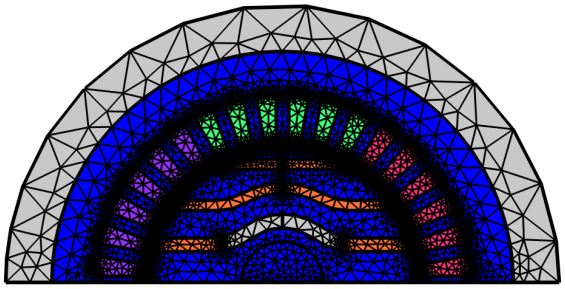

Figure 6. Mesh used in the Finite Element model.

3.3. Validation

For the whole validation, the model with three layers per rotor bar is used to account for skin effect. This is why FEM also has three rotor circuits accounting for three end ring layers. Furthermore, at first all iron ribs of the rotor are set to air (as for the model) in order to validate that the model is correct and to see the difference already occurring if the geometry is the same.

At first, an unsuccessful start-up at 140 V is shown (Figure 8). The results for the speed show that the acceleration phase from start to 0.4 s slightly differs because the slope in the model is lower than in FEM. This can be explained by the fact that the saturation factors for the model are evaluated for synchronous speed and cannot consider for accurate saturation states at low speeds. But apart from that the model provides good results for the steady state starting from 0.4 s since the speed oscillations show a good agreement with FEM. This is the most important because this region close to synchronous speed decides whether the machine synchronizes or not. Since the saturation state is close to no-load conditions and the model to consider for skin effect in the rotor cage is accurate enough, the final speed is the same as for FEM. The stator current also fits good regarding the amplitudes.

In the next step, we want to let the machine synchronize which is why the voltage is increased to 180 V. Figure 9 shows that again the speed versus time curve of the model fits FEM quite well as does the stator current. The only difference apart from the slope that can be observed is that the speed oscillations in the model are less damped than in FEM. Since we still focus on the fact that the machine synchronizes and the overall behavior fits good, we can consider this result as satisfactory.

Now that the model is validated for the case that the rotor

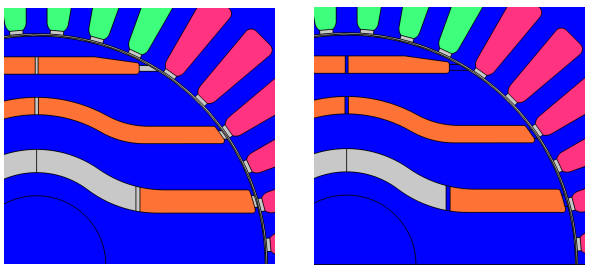

(a) ribs set to air (b) ribs set to iron

Figure 7. Finite Element model with different material for the inner and outer mechanical ribs and bridges.

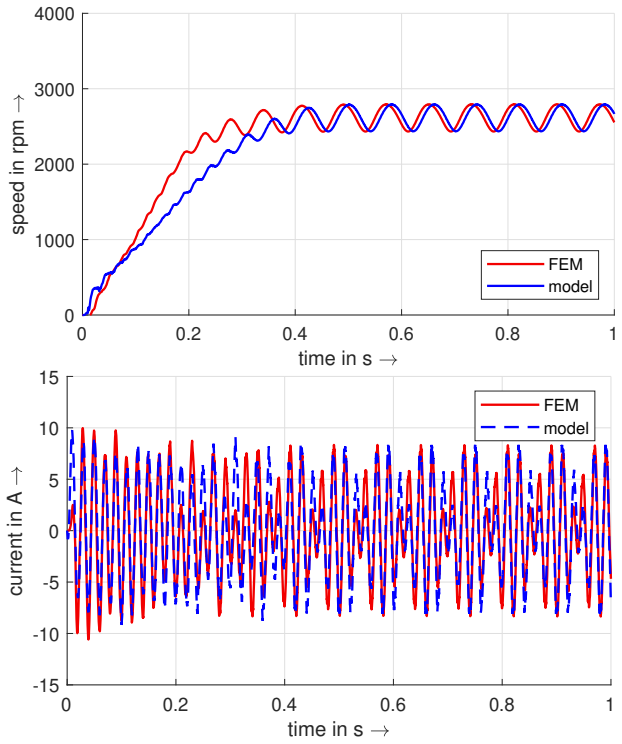

Figure 8. Speed (top) and stator current of phase 1 (bottom) during the unsuccessful start-up at 140 V. Ribs and bridges are set to **air** in both models.

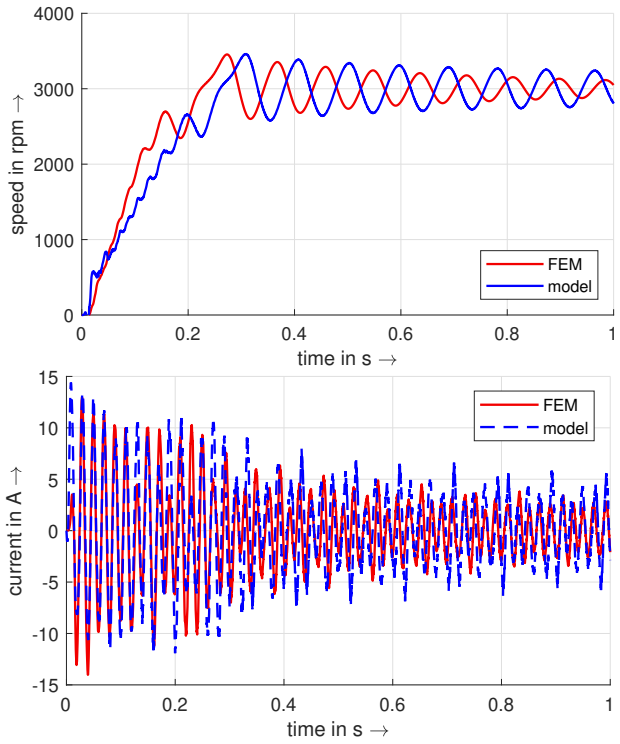

Figure 9. Speed (top) and stator current of phase 1 (bottom) during the successful start-up at 180 V. Ribs and bridges are set to **air** in both models.

ribs and bridges are air, we can set their properties to iron (Fig. 7). For this, we need a new calculation of lookup tables for the saturation factors, where in the nonlinear reference the material of the ribs is adapted. Figure 10 shows the results for this case.

Even here we can observe a good agreement between the model and FEM. What stands out is that the model has a phase of almost constant speed between 0.4 and 0.6 seconds. This is due to the fact that because of the different acceleration phases, FEM and the model have different rotor positions in relation to the voltage close to synchronous speed. In case of the model this means that the behavior here looks slightly different. But if the combination of rotor angle and voltage angle would be the same for FEM, the curve would show the same behavior. Furthermore, the damping in the model is again a bit different from FEM.

Whats interesting to mention as well is that the currents are lower than in the first comparisons and the machine pulls into step for a voltage that would not reach synchronism if the ribs were set to air (cf. Fig. 8). This can be explained by the smaller carter factor that is achieved when the rotor has no slots which improves mainly the d-axis inductance and thus the torque.

4. DISCUSSION

All in all the results look good and prove that the model is quite promising for achieving the goal of a faster computation of start-ups than with FEM.

Concerning the computation times, the model with three rotor bar layers requires 2:09h for the preliminary calculations (inductances, resistances, saturation factors). After that, the simulation of the start-up procedure requires less than a minute (47 s for Fig. 8). Even though in total this seems quite high at a first glance, every further start-up simulation for the same machine is now very fast (46 s for Fig. 9) because now the model paramters are known. In contrast, FEM with three rotor bar layers (i.e. three rotor circuits instead of one) takes 6:22h and 6:31h which sums up to almost 13 hours for both calculations. Even with the standard model of one rotor circuit, it would still last more than 3:30h. This means that for every further calculation (for example with another voltage, stator or rotor resistance, etc.) we are saving even more time.

We can see that the basic approach that considers for skin effect together with a simplified approach for saturation by saturation factors tremendously reduces the amount of preliminary time-consuming calculations. A disadvantage of the model that has to be mentioned is the need for opening the iron ribs and bridges in the model. This causes the space harmonics to be higher than in reality since the slots in the air-gap are already opened at low saturation states. The torque ripple will therefore be overestimated in many cases. Hence, a good 'virtual' slot has to be found which fits the saturation states of the real machine better. The fundamental current however is considered for by the saturation factors. This topic will be studied in detail in future work. The validation of both models with measurements of different machines will be published as well.

5. ACKNOWLEDGEMENTS

This work was supported in part by the PROCOPE mobility grant from the Department for Science and Technology of the French Embassy in Germany.

6. REFERENCES

[1] The European Commision, "Commision Regulation (EU) 2019/1781," *Official Journal of the European Union*, vol. 72, pp. 74–94, Oct. 2019.

[2] V. Abramenko, J. Bárta, I. Lolová, I. Petrov, and J. Pyrhönen, "Design of a low-power direct-on-line synchronous reluctance motor based on the modified natural flux line curve approach," *IEEE Transactions on Industry Applications*, vol. 57, no. 6, pp. 5894–5906, 2021.

[3] M. Villani, M. Santececca, and F. Parasiliti, "High-efficiency line-start synchronous reluctance motor for fan and pump applications," in *2018 XIII International Conference on Electrical Machines (ICEM)*, 2018, pp. 2178–2184.

[4] M. Gamba, G. Pellegrino, A. Vagati, and F. Villata, "Design of a line-start synchronous reluctance motor," in *2013 International Electric Machines & Drives Conference*, 2013, pp. 648–655.

[5] M. Muteba, "Line-start synchronous reluctance motor with v-shaped rotor laminations," *IEEE Access*, vol. 10, pp. 109 277–109 288, 2022.

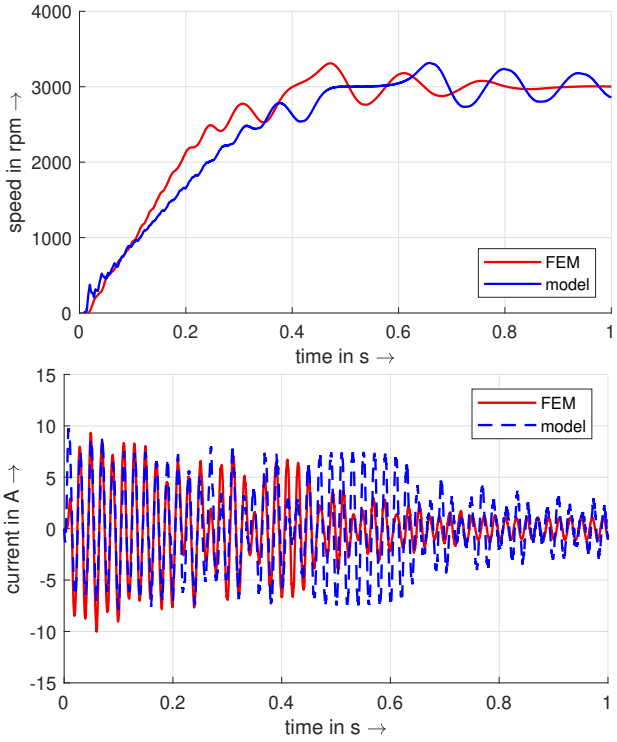

Figure 10. Speed (top) and stator current of phase 1 (bottom) during the successful start-up at 140 V. Ribs and bridges are set to **iron** in both models.

[6] J. Güdelhöfer, R. Gottkehaskamp, and A. Möckel, "Transient Model of Direct on Line Induction and Synchronous Reluctance Motors with Inter-bar Currents," in *2018 XIII International Conference on Electrical Machines (ICEM)*, 2018, pp. 440–446.

[7] J. Güdelhöfer, "Analytisches transientes Berechnungsmodell für selbstanlaufende Synchronreluktanzmaschinen," Ph.D. dissertation, Karlsruhe Institute of Technology (KIT), Karlsruhe, 2019.

[8] S.-A. Tahan and I. Kamwa, "A two-factor saturation model for synchronous machines with multiple rotor circuits," *IEEE Transactions on Energy Conversion*, vol. 10, no. 4, pp. 609–616, 1995.

[9] J. Rituper, J. Güdelhöfer, and R. Gottkehaskamp, "Consideration of the Skin Effect in a Transient Model of Line-Start Synchronous Reluctance Machines," in *2020 International Conference on Electrical Machines (ICEM)*. IEEE, 8232020, pp. 97–103.

[10] L. Quéval and H. Ohsaki, "abc-modeling of permanent magnet machines using n-d lookup tables: a finite element validation," in *Symposium de génie électrique (SGE'2014)*, 2014.

[11] L. Queval and H. Ohsaki, "Nonlinear abc-Model for Electrical Machines Using N-D Lookup Tables," *IEEE Transactions on Energy Conversion*, vol. 30, no. 1, pp. 316–322, 2015.

[12] J. Rituper and R. Gottkehaskamp, "Consideration of the saturation in a transient model of line-start synchronous reluctance machines," in *2022 International Conference on Electrical Machines (ICEM)*, 2022, pp. 62–68.

[13] P. Lombard and F. Zidat, "Determining end ring resistance and inductance of squirrel cage for induction motor with 2d and 3d computations," in *2016 XXII International Conference on Electrical Machines (ICEM)*, 2016, pp. 266–271.